Passive and Active Hybrid Integrated EMI Filters

Juergen Biela, *Member, IEEE*, Alexander Wirthmueller, Roman Waespe, Marcello Lobo Heldwein, *Member, IEEE*, Klaus Raggl, *Member, IEEE*, and Johann W. Kolar, *Senior Member, IEEE*

***Abstract*—Two new planar integrated electromagnetic interference (EMI) filter structures that reduce the filter volume and that are based on standard printed circuit board (PCB) process technology are presented in this paper. First, a passive integrated EMI filter is presented, which results in a volume reduction of 24% compared to the discrete solution. However, this filter requires a planar ferrite core for the common-mode inductor. In order to eliminate the ferrite core and reduce the filter volume further (−40% versus discrete filter), a passive integrated structure is combined with an active EMI filtering circuit. The transfer function, the volume, and the losses of the discrete and the two integrated filters, which are designed for a 600 W power-factor-corrected converter, are compared.**

***Index Terms*—Active filter, electromagnetic interference (EMI) filter, integrated passives, printed circuit board (PCB) inductor.**

I. Introduction

THE PURSUIT of obtaining higher power density ac/dc and dc/dc converters leads to increasing switching frequencies in order to reduce the size of the energy storage elements. These energy storage elements usually influence the overall size of a converter significantly. This has resulted in the development of electromagnetically integrated structures [1] that combine several functions in one passive component.

Due to increasing switching frequencies, conducted emissions from 150 kHz to 30 MHz have increased. Thus, the electromagnetic interference (EMI) filter has also become a significant part of the converter in terms of size and cost. For this reason, some electromagnetically integrated EMI filter structures [2] and [4] and also active EMI filters [5] and [6] have been proposed.

In this paper, two new planar EMI filter structures are presented that allow a significant reduction of the filter volume. These structures are integrated in a printed board circuit (PCB), which could be manufactured using a cost-saving standard PCB manufacturing process.

Manuscript received October 2, 2008; revised November 20, 2008. Current version published May 6, 2009. This paper was presented in part at the Applied Power Electronics Conference and Exposition (APEC), Dallas, TX, February 2006. Recommended for publication by Associate Editor P. Tenti.

J. Biela, R. Waespe, K. Raggl, and J. W. Kolar are with the Power Electronic Systems Laboratory, Swiss Federal Institute of Technology Zurich (ETH Zurich), Zurich 8092, Switzerland (e-mail: biela@lem.ee.ethz.ch; waesper@ee.ethz.ch; kolar@lem.ee.ethz.ch).

A. Wirthmueller was with the Power Electronic Systems Laboratory, Swiss Federal Institute of Technology Zurich (ETH Zurich), Zurich 8092, Switzerland. He is now with Columbia University, New York, NY 10027-70031 USA (e-mail: awirthm@gmail.com).

M. L. Heldwein is with the Federal University of Santa Catarina, Florianopolis 88040-970, Brazil (e-mail: heldwein@inep.ufsc.br).

Color versions of one or more of the figures in this paper are available online at http://ieeexplore.ieee.org.

Digital Object Identifier 10.1109/TPEL.2009.2012404

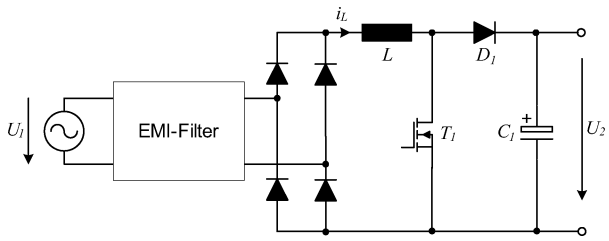

Fig. 1. Circuit diagram of a 600 W PFC.

TABLE I
SPECIFICATION OF PFC CONVERTER

Parameter	Value
Output Power	600W
Output Voltage	410V
Switching Frequency	250kHz
Input Voltage	110V - 230V
(incl. tolerances)	(93V - 264V)
Input Current	2.6A - 5.5A
(incl. tolerances)	(2.3A - 6.5A)

With the first filter structure, all inductor windings and all capacitors except for a large differential-mode (DM) capacitor are integrated in the PCB. The DM capacitor is realized by a parallel connection of X2 SMD-X7R capacitors. For the large inductance value of the common-mode (CM) choke, a planar ferrite core is needed, although the overall filter has a very low profile (height <9.5 mm) and a low volume (≈25% volume reduction in comparison to a discrete solution). This filter is called a passive hybrid integrated EMI filter due to the combination of integrated and discrete passive components.

In a second step, the passive integrated structure is combined with an analog amplifier (active EMI filter). With the amplifier stage, the required inductance and capacitance values of the components decrease significantly, so that no additional ferrite core is needed. The components of the active filter are mounted on top of the PCB, where the passive filter is integrated. This new approach results in a very compact construction (≈40% volume reduction in comparison to a discrete solution) and is called active hybrid integrated EMI filter.

The two proposed filter structures are designed for a 600 W power-factor-corrected (PFC) converter intended for information technology (IT) applications (cf., Fig. 1) with the specification given in Table I. In Section II of this paper, the discrete EMI filter for the PFC converter is described for comparing the new structures with a conventional filter. The structure of the passive

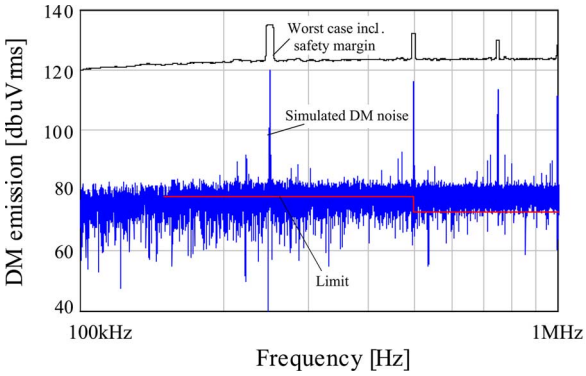

Fig. 2. Simulated emission levels of DM noise, worst-case values inclusive of 6 dB safety margin, and limit values (light-colored curve: CISPR 11 class A QP limit).

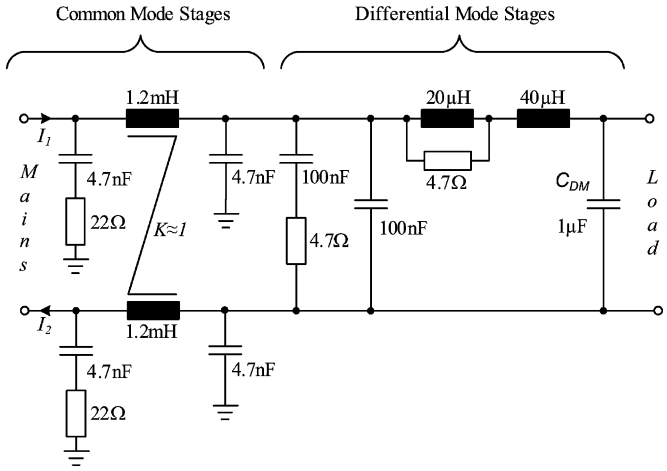

Fig. 3. Circuit diagram of the discrete EMI filter.

hybrid integrated EMI filter, which is designed and optimized using finite-element method (FEM) simulations, is presented in Section III. Thereafter, the mode of operation and the design of the active hybrid integrated EMI filter is explained in Section IV. The measured transfer functions of all three filters together with the losses/efficiency and the volume are compared in Section V. Finally, a conclusion and topics of future research are given in Section VI.

II. Discrete EMI Filter

The discrete EMI filter is designed according to the procedure described in [10] and [11], which is summarized shortly in the following. First, the DM- and CM-conducted emissions of the PFC converter are calculated by simulating a high-order circuit model including the relevant parasitic elements. The resulting DM emission levels are given as an example in Fig. 2, where the blue line describes the simulated emission level measured by the line impedance stabilization networks (LISN), the black curve represents the worst-case maximum values inclusive of safety margin, and the red and the green line the limits.

With the DM noise and the regulations on conducted RF emissions for the intended application [Special International Committee on Radio Interference (CISPR) 11], the required attenuation of the DM filter could be calculated by selecting the largest peak value within the relevant range (150 kHz–30 MHz) and comparing this value to the limits. The required filter attenuation is used to choose an appropriate DM filter topology [9] and the number of connected filter stages in series. On the basis of the filter topology, the corner frequency of the filter is calculated, so that the attenuation is equal to the required one plus 6 dB margin at the given frequency. With the corner frequency of the filter, the LC products are given. The filter damping is—among other things—determined by an upper limit for the output impedance of the filter. This limit is given by the control loop of the PFC converter since the output impedance influences the stability of the system. The controller regulates the dc output voltage to a constant voltage resulting in a constant power load behavior at the input. This behavior could lead to instabilities in combination with the mains/EMI filter impedances [12], [13].

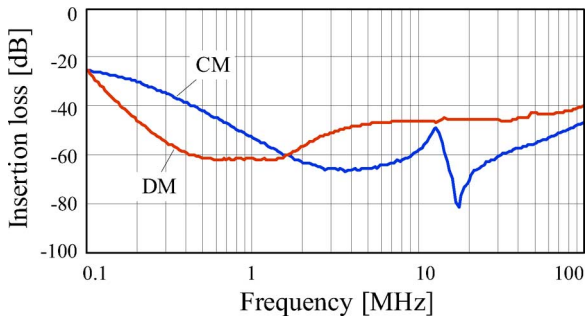

Fig. 4. Insertion loss of the discrete EMI-filter.

Now, the filter topology for the DM, the corner frequencies, and the required damping are known. Depending on the number of filter stages and the topology, there are some DOFs for the choice of the component values. These degrees of freedom are used to minimize the overall volume of the DM EMI filter.

As with DM noise, the required attenuation for the CM could be calculated from CM noise simulation and given limits. With the required attenuation, the filter topology is selected and the corner frequency of the filter is calculated. Since the Y-capacitor size is limited by the regulations—the current to ground must not exceed 3 mA at 50 Hz—the value of the inductance is determined for Y-capacitor values close to the maximum allowed ones according to electrical safety regulations. In order to damp the CM filter properly, some resistors in series with the capacitors are added.

The resulting filter topology and the component values are shown in Fig. 3. For the CM choke, Vitroperm from Vacuumschmelze has been chosen in order to minimize the inductor volume. The measured insertion loss of the discrete filter is shown in Fig. 4 and the design of the filter is shown in Fig. 5, and the overall volume is 47.4 cm^3 (48 mm $\times$ 38 mm $\times$ 26 mm). In the next step, integrated filters with comparable performance are designed.

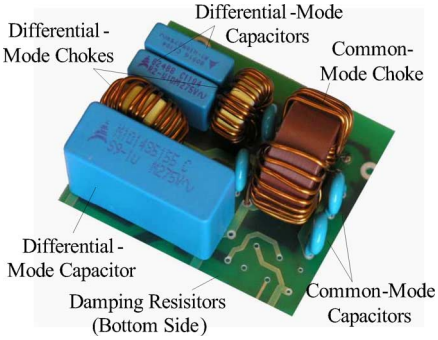

Fig. 5. Photograph of the discrete EMI filter.

TABLE II
PARAMETERS OF THE PASSIVE HYBRID EMI FILTER

Parameter	Value
DM Inductance	182 μH
Number of turns	17
Coupling factor	0.86
Loss @110V in DM choke	17.8 W
CM Inductance	1.5 mH
Number of turns	16
Loss @110V in CM choke	8.4W
Size [mm]	80×80×7.2
Boxed volume	46.1 cm^3

III. PASSIVE HYBRID EMI FILTERS

In order to reduce the filter volume and simplify the manufacturing, the discrete EMI filter components are—if possible—integrated into a PCB, which could be manufactured with state-of-the-art PCB process technology. The circuit diagram of the passive hybrid integrated EMI filter is shown in Fig. 6(a) and the filter parameters are given in Table II.

In comparison to the discrete filter, the DM inductors are arranged symmetrically in the lines and the DM inductance value is slightly larger. This results in smaller CM capacitors (100 nF/800 nF instead of 100 nF/1 μF) for the same corner frequency of the DM filter.

The assembly of the passive hybrid filter is shown in Fig. 6(b). Each of the coupled DM inductors is integrated by four 105-μm copper layers, which are connected in parallel in order to minimize the ohmic losses. The copper layers are covered on both sides by a 1.25-mm-thick layer of FPC 351 (Epcos, [14]). Each coil consists of 17 turns, which are arranged at the edge of the 80 mm × 80 mm PCB. The total width of the coils is 20 mm. Thus, there is a 40 mm × 40 mm large region in the center of the board where the winding of the CM choke could be integrated, as shown in Fig. 6(b). Due to the large CM inductance, a planar electroluminescent panel (ELP) 32 core is used for the CM inductor. The DM coils use two FPCs and one μ-metal (Vacuum Atmosphere Company (VAC) [15]) layer as magnetic path.

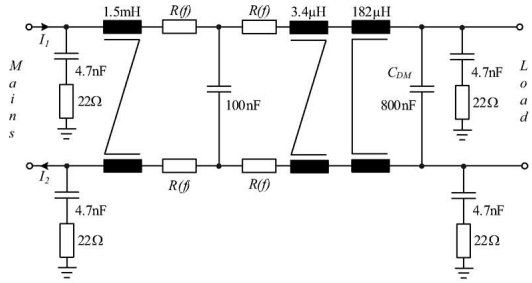

(a)

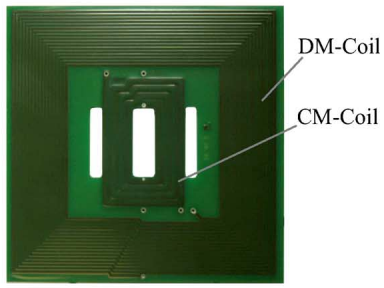

(b)

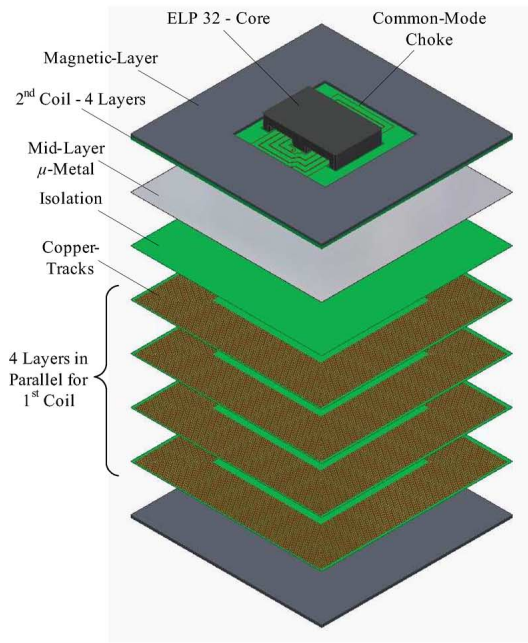

(c)

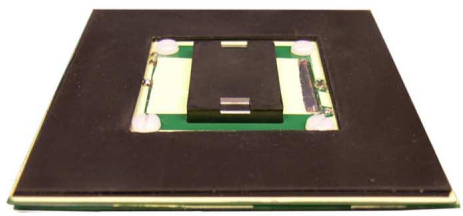

(d)

Fig. 6. (a) Circuit diagram of passive integrated filter. (b) Photograph of four-layer PCB for one DM (two are need for the passive filter). (c) Layer stack of passive integrated filter. (d) Photograph of assembled passive hybrid filter.

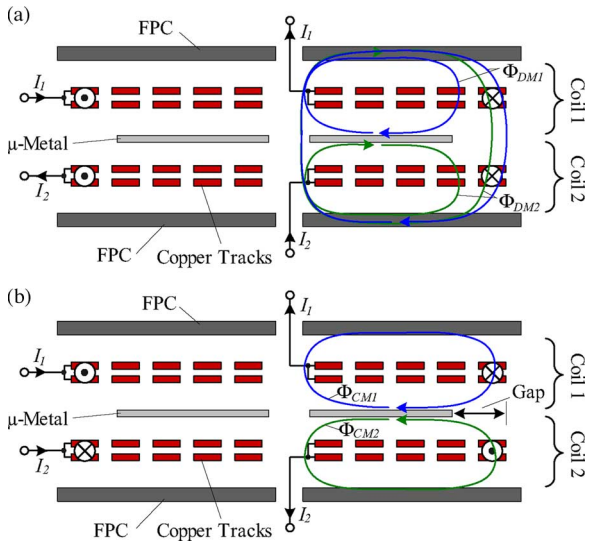

Fig. 7. (a) Diagram of coupled coils. (b) Design of the coils.

The damping of the passive integrated filter mainly results from the frequency-dependent resistors $R(f)$, which represent the high-frequency losses of the coils due to skin and proximity effect. The geometry of the coils is designed so that the dc losses are low, but the high-frequency losses are high enough to damp the filter. The damping elements at the input and output of the filter remain in order to attenuate oscillations caused by the line or the input impedance of the converter. The capacitors and the resistors of the damping elements could also be integrated in the PCB using dielectric and resistive layers (e.g., HiK-material and OHMEGA-PLY/Carbon Paste, respectively [16], [17]). In order to simplify the testing of the filter, the capacitors and resistors of the damping network are realized by surface mount device (SMD) components in the prototype.

A. *Design of Coupled Inductors*

The symmetrically arranged DM inductors are implemented by two coupled inductors. In Fig. 7, the principle of operation is shown for DM excitation in Fig. 7(a) and for CM excitation in Fig. 7(b) (PCB cross section with two parallel layers each).

The assembly of the coupled coils consists of the following five different layers:

1) magnetic layer at the top (e.g., Mag–Lam [3], FPC, μ-metal)—thickness: $\sim$1 mm;
2) winding of coil 1 consisting of one or more copper layers connected in series and/or parallel;
3) thin layer ($\sim$100 μm) of magnetically and electrically conductive μ-metal (comparable to silicon steel);
4) winding of coil 2 (usually, same design as coil 1 but reverse winding direction);
5) magnetic layer at the bottom (same as at the top).

In Fig. 7(a), the current and the flux direction in the coils for DM excitation are shown. The current I_1 in the upper coil causes the magnetic flux Φ_{DM1} and the current I_2 in the lower coil Φ_{DM2}. In the μ-metal layer in the middle, both DM fluxes cancel each other (dashed lines) so that there is no flux in the

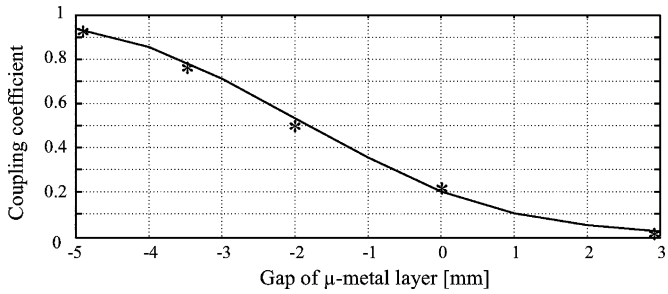

Fig. 8. Dependence of the coupling factor k on the length of the μ-metal layer (cf. Fig. 7)—measured values at *.

μ-metal layer for a symmetric design under DM excitation. Consequently, the value of the DM inductance of the integrated coils is independent of the size of the μ-metal layer.

In Fig. 7(b), the current direction and flux distribution for CM excitation are given. Due to symmetry reasons, the CM flux of both coils Φ_{CM1} and Φ_{CM2} adds up and flows in the middle between the two coils through the gap and the μ-metal layer. The shorter the gap is, the lower the magnetic reluctance of the path is and the higher is the CM inductance.

The ratio between the DM and the CM inductance values defines the coupling between the two coils (the larger the $L_{\mathrm{CM}}/L_{\mathrm{DM}}$, the lower is the coupling—by reducing the coupling, mainly the CM inductance of the integrated structure is increasing, while the DM inductance is approximately constant). This relation is controlled by the horizontal extension of the μ-metal layer. If this layer starts at the very left side and ends at the very right side of the coil, the coupling is approximately zero. In Fig. 8, the dependence of the coupling factor k on the length of the μ-metal layer is shown for a test assembly. These results have been obtained by the developed design procedure (described later) and are validated by measuring the coupling coefficient for different extensions of the μ-metal layer.

Since the CM current/flux has almost no spectral components below the switching frequency, the amplitude of the CM flux is small. Therefore, the μ-metal layer, which has a saturation flux density of approximately 0.8 T, could be very thin ($\approx$100 μm).

The distributed capacitance between a winding and a conductive layer is transformed into a network consisting of three capacitors (cf. Fig. 9) in [18]. The capacitance C is the static capacitance between the winding and the conductive layer (cf. [19]). As the equivalent capacitance parallel to the winding is negative, it could be used to cancel the parasitic capacitance C_P of the winding (cf. [4] and [8]). Thus, the distributed capacitance caused by the μ-metal layer could be used to reduce the value of the capacitance in parallel to the winding and to increase the frequency of the first resonance of the coil if the layer is connected to the ground. The value of the static interlayer capacitance C is calculated within the design procedure and adjusted by varying the vertical distance between the μ-metal layer and the winding.

With the construction shown in Fig. 7, where the CM flux flows through the μ-metal layer in the middle, the DM inductance is larger than or equal to the CM inductance due to the coupling of the DM flux. If a larger CM inductance and a lower

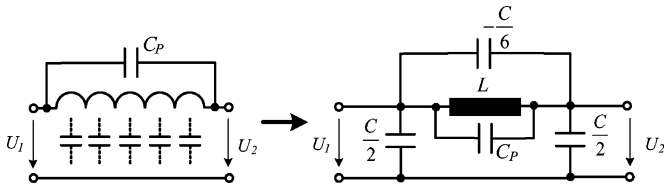

Fig. 9. Equivalent network for a distributed capacitance between a winding and a conductive layer according to [18].

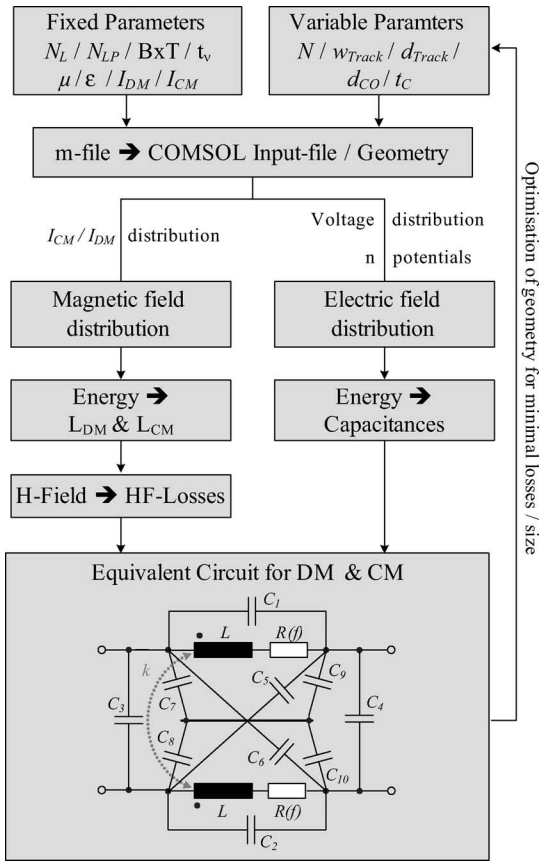

Fig. 10. Flowchart of the design procedure for the integrated coils.

DM inductance are needed, the winding direction of one coil has to be changed. In this case, a thicker magnetic middle layer (twice the thickness of the outer magnetic layer) is needed, because the relatively large DM flux flows through the middle layer. The achievable maximum values for the CM and the DM inductances are the same for both design possibilities, if the distance between two magnetic layers above and below one PCB (i.e., the gap) is the same. Consequently, the design with the changed winding direction leads to an increased volume and larger magnetic losses for the same maximum achievable inductance values, and should only be used in case a CM inductance is needed, which is larger than the DM one.

B. Design Procedure

The integrated inductors of the EMI filter are designed using an automated design procedure, whose flow chart is given in Fig. 10. This procedure, which is based on FEM simulations

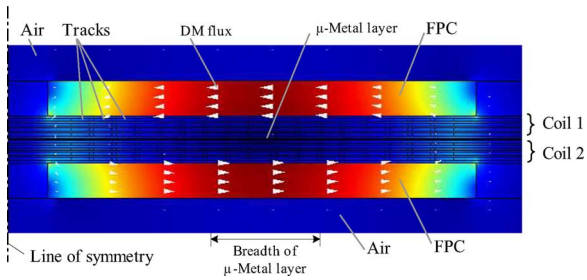

Fig. 11. DM—finite-element simulation of passive hybrid integrated EMI filter.

(COMSOL) and analytic calculations, will be shortly explained in the following.

At the beginning of the procedure, different parameters like the number of layers in the PCB N_L, the number of parallel connected layers N_{LP}, PCB size $B \times T$, the vertical distance between the layers t_ν, etc., must be specified by the user. These parameters are not varied within the design procedure since they mainly depend on requirements not related to the filter itself. On the other hand, there are parameters like the number of turns N, the PCB width w_{Track} and distance w_{Track}, the thickness t_C of the magnetic layers, etc., which could be varied in order to optimize the design.

With the parameters given in MATLAB, input files for FEM simulations describing the geometry and boundary conditions are automatically generated by the program. In the next step, FEM simulations are carried out by the program for different setups (CM and DM excitation, different voltage distributions)—cf. Fig. 11. On the basis of the magnetic and electric energies, the inductance and capacitance values are calculated. Furthermore, the magnetic field distribution is used to calculate the HF resistances of the coils analytically. Thereafter, the calculated values are transformed into equivalent circuit values of the EMI filter.

The described design routine offers the possibility to be used within an optimization routine, which varies, for example, the number of turns and the design of the tracks in order to minimize the filter volume or maximize the efficiency.

IV. Active Hybrid EMI Filter

The discrete and also the passive hybrid EMI filters require a large CM inductance because the value of the Y-capacitance is limited by regulations and the corner frequency of the filter is low due to the CM emission level. Since the amplitude ratio of the high-frequency CM current and the DM current at the line frequency is usually relatively small, the volume of the CM inductor could be reduced by using an active filter. This active EMI filter consists of two small CM inductors, two 20 nF capacitors, a measurement network, and an analog amplifier, as shown in Fig. 12(a) (cf. [20]).

With the measurement network, the CM voltage V_{CM} caused by the converter/load is measured via the two 1-nF capacitors. The CM voltage is amplified by an analog class-A amplifier, which injects an inverted CM current via the two 22-nF capacitors into the filter network. Thus, the CM current resulting

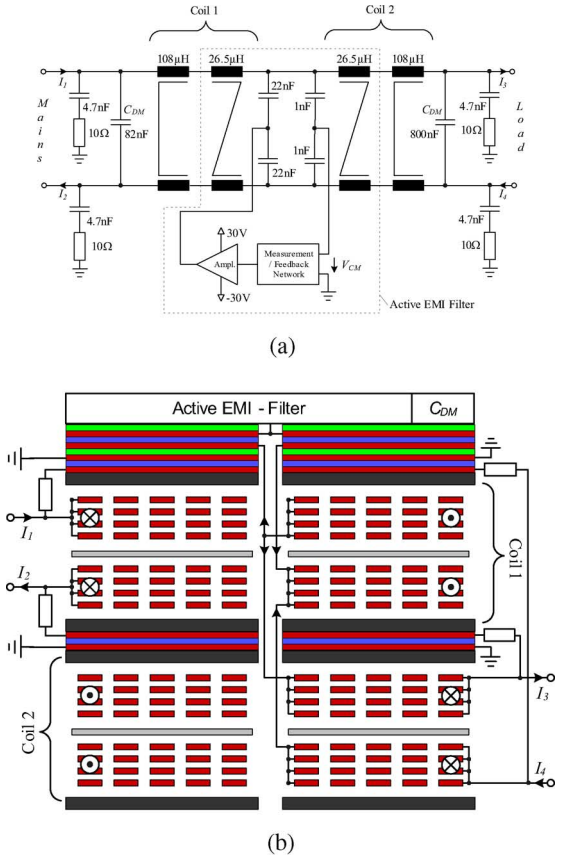

Fig. 12. (a) Circuit diagram of the active hybrid integrated EMI filter. (b) Design of the active hybrid integrated EMI filter.

TABLE III
MATERIALS FOR CAPACITANCE INTEGRATION

	C-Lam	HiK	Rogers
Permittivity	11		10.2
Breakdown Voltage	30kV/mm	1kV	-
$\tan\delta$	0.02	0.02	0.0027
Capacitance per cm^2	0.2nF	0.2nF	0.2nF

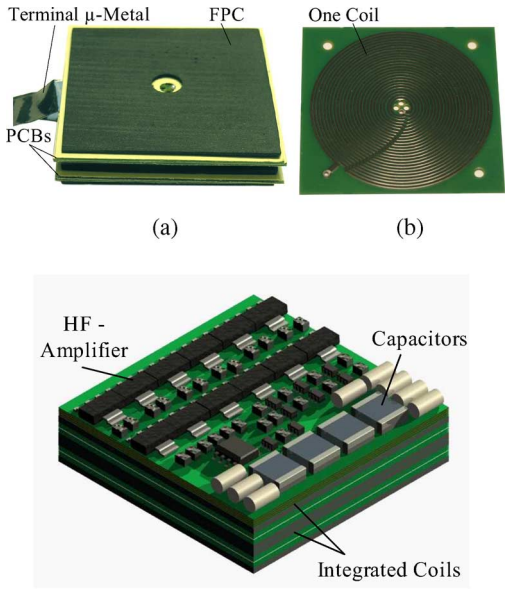

Fig. 13. (a) Picture of assembled active hybrid EMI filter. (b) Picture of the PCB of one layer. (c) 3-D drawing of final assembly of active filter.

from the load is canceled/reduced by the active filter. Due to the limited gain of the amplifier and nonideal components, the amplitude of the CM voltage/current is only reduced by approximately 20 dB in the best case.

Moreover, the limited bandwidth of the amplifier requires a reduction of the gain at higher frequencies in order to guarantee the stability of the system. This also results in a decline of the CM voltage/current cancelation at higher frequencies. In the limited frequency range from approximately 100 kHz up to 6 MHz, where the voltage/current cancelation is working, the effective CM capacitance is increased very much by the amplifier. Thus, a smaller CM inductance can be used to obtain the same corner frequency/attenuation as for the CM filter of the discrete/passive hybrid filter.

The decline of the attenuation due to the limited amplifier bandwidth is not critical, because the effective impedance of a large CM choke also decreases with increasing frequency due to the parasitic capacitance that causes a parallel resonant behavior of the choke at higher frequencies.

The two CM inductors needed for the active EMI filter are integrated in the PCB, as described in the previous section. The final design of the complete active hybrid integrated filter is shown in Fig. 12(b), where the components of the active filter are mounted on top of the PCB. Below the active filter, the capacitances for measuring the CM voltage and injecting the CM current as well as the relatively small capacitances for damping resonances at the input and the output of the filter can be integrated. Due to the planar design, these capacitors show low equivalent series resistance (ESR) and equivalent series inductance (ESL). In Table III, some dielectric materials for integrating capacitances into PCBs are shown.

Due to the relatively low permittivity of these materials, the large capacitors for the DM $C_{\rm DM}$ still have to be realized as SMD capacitors that are mounted on top of the PCB besides the active filter components.

In Fig. 13(a), the examined prototype of the coupled coils for the active filter is shown. It consists of four layers of FPC 302 from Epcos with a thickness of approximately 1.3 mm, four PCBs, each with four 105 μm layers of copper for the coils [cf. Fig. 13(b)], and two layers of μ-metal. On the left-hand side, the terminals of the μ-metal layers are shown with which the layers could be connected to ground in order to reduce the parasitic capacitance. Below the pictures, a 3-D drawing of the final assembly of the integrated active hybrid filter is shown in Fig. 13(c). In Table IV, the technical parameters of the active EMI filter are listed.

TABLE IV
PARAMETER OF ACTIVE HYBRID EMI FILTER

Parameter	Value
DM Inductance	216 μH
CM Inductance	53 μH
Losses @ 110V	28.4 W
Size [mm]	60×60×16.2
Volume	27.3 cm^3

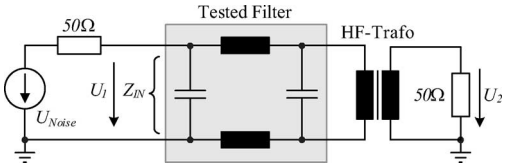

Fig. 14. Circuit for the measurement of the transfer (U_2/U_1) function (filter attenuation) and the input impedance.

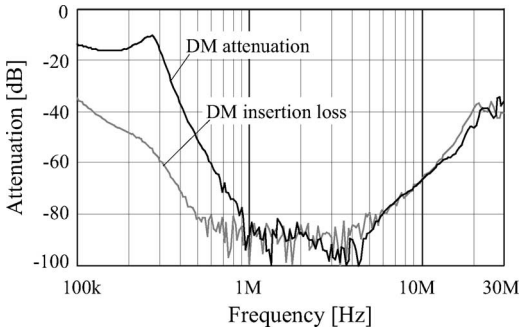

Fig. 15. Comparison between the DM attenuation/transfer function (U_2/U_1) and insertion loss of the active hybrid filter.

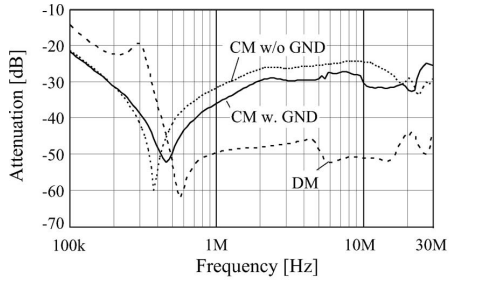

(a)

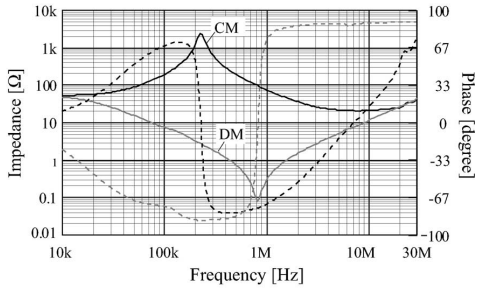

(b)

Fig. 16. (a) Transfer function of the passive filter for CM with (with GND) and without connection of the μ-metal layer to ground (without GND) and for DM. (b) Input impedance of the filter at the load side for CM and DM with phase (dashed lines).

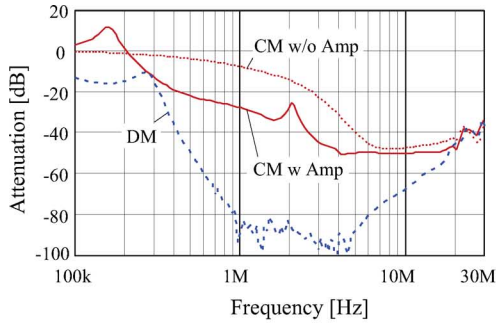

(a)

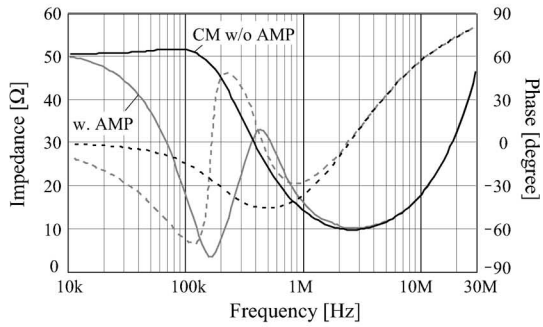

(b)

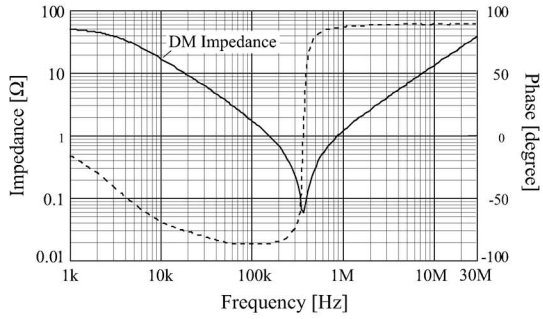

(c)

Fig. 17. (a) Transfer function of the active filter for CM with (with AMP) and without amplifier (without AMP) and for DM. (b) Input impedance of the filter at the load side for CM with (with AMP) and without amplifier (without AMP) with phase (dashed lines). (c) Input impedance of the filter at the load side for DM with phase (dashed lines).

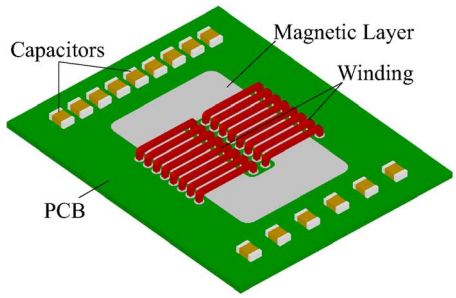

Fig. 18. New design of the CM choke.

V. COMPARISON OF THE EMI FILTERS

In order to compare the performance of the different filters, measured transfer functions, losses, and volume of the discrete, the passive, and the active hybrid filters are presented in the following.

TABLE V
CALCULATED AND MEASURED PARAMETERS OF THE THREE COMPARED EMI FILTERS

Parameter	Discrete Filter	Passive Filter			Active Filter		
		calculated	measured	modified	calculated	measured	modified
DM Inductance	60 μH	194 μH	182 μH	206 μH	132 μH	108 μH	150 μH
CM Inductance	1.2 mH	1.45 mH	1.5 mH	1.45 mH	65 μH	53 μH	73 μH
Losses @7.7A$_p$/110V	3.56 W	2x(7.6+3.7)W	2x(8.9+4.2)W	2x(2.2+3.7)W	4x5.7W+6W	4x7.1W+6.1W	4x1.6W+6W
Efficiency @110V	99.4 %	96.2 %	95.6 %	98 %	95.2 %	94.3 %	98 %
Efficiency @230V	99.8 %	99.1 %	99.0 %	99.5 %	98.1 %	97.9 %	98.8 %
Total Volume	47.4 cm^3	-	36.1 cm^3	27.4 cm^3	-	27.3 cm^3	21.3 cm^3

Usually, insertion loss measurements, i.e., the ratio U_2/U_{Noise}, are used to characterize EMI filters. However, these measurements also include the attenuation that results from the source impedance of the measurement circuit (usually 50 Ω) and the filter capacitors (cf. Fig. 14). The source/internal impedance of the noise source and also the additional attenuation depend very much on the converter topology and the design of the converter. In order to obtain information about the filter attenuation that is independent of the source impedance, the transfer function, i.e., the ratio U_2/U_1, is used in the following. The input voltage of the filter U_1 for a given source impedance could be calculated with the input impedance Z_{IN} of the EMI filter, which is also presented in the following. The additional attenuation because of the source impedance could be seen in Fig. 15, where the DM insertion loss and the transfer function for the active filter are plotted in the same graph.

In Fig. 16, the CM and the DM attenuation and the input impedance of the passive hybrid filter are given, where the two curves for the CM show the different attenuation of the filter when the μ-metal layer is connected to ground or free floating. Due to the additional parasitic capacitances (cf. Fig. 9), the HF behavior of the filter is improved. The resonant peak of the CM attenuation between 400 and 500 kHz results from the characteristic frequency of the CM choke.

Due to the large source impedance of the PFC converter (boost inductor: 187 μH—cf. Fig. 1), the DM attenuation of the passive filter increases very much in the frequency range from 100 kHz to 1 MHz, since the input impedance of the filter is relatively low in this region. For example, at 100 kHz, approximately additional 20 dB results from the large source impedance resulting in an effective attenuation larger than 40 dB for DM at 100 kHz.

In the considered frequency range, the input impedance of the active filter for DM is even lower than that of the passive filter, which leads to a larger additional damping due to the source impedance (cf., Fig. 17). Consequently, the DM attenuation of the two integrated filters is comparable to that of the discrete filter and even exceeds it a bit.

The comparatively low resonance frequency of the CM choke of the passive integrated filter results in a CM attenuation curve that is not as good as that of the discrete filter. The reason for this is the parasitic capacitances resulting from the planar winding design. A possible alternative design of the CM choke, which leads to reduced parasitic capacitances and also lower losses, is shown in Fig. 18, where the core is integrated in the PCB by magnetic layers and the winding consists of wire or in case of low-power applications of PCB tracks. For the considered 600-W PFC system, the winding must be made of wires in order to keep the efficiency high. Since this would require special manufacturing technologies, which are out of the focus of this project, this approach is not further investigated.

In Fig. 17(a), the CM attenuation of the active integrated filter is shown, where it could be seen that the amplifier results in an additional attenuation of 15–20 dB in the frequency range from 400 kHz to 4 MHz. The resonant peak at approximately 160 kHz is caused by the limited gain of the amplifier. As simulations show, the gain could be increased by using transistors with a higher transition frequency in the power stage of the amplifier.

The resonant peak around 2 MHz in the CM attenuation of the active integrated filter is caused by the characteristic frequency of the integrated coils.

In Table V, the volume, the losses, and the efficiency of the three EMI filters are given. The values in the "modified" columns result from using Vacoflux 48 (VAC [15]), which has a saturation flux density of 2 T, instead of FPC 351/302 [14] as the magnetic layer. The basic design of the inductors is the same for both materials, just the higher possible maximal flux density is utilized to reduce the number of turns and therewith the losses. As can be seen, the losses and the volume of the integrated filters can be reduced very much so that the efficiency of the integrated filters is comparable to that of the discrete filter, but the volume is reduced by more than 40%.

The presented approach for the passive hybrid filter, which is the more promising integration method if burst test and high-voltage spikes at the mains are considered, is also applied to an

TABLE VI
PARAMETER OF THE 300W PASSIVE HYBRID EMI-FILTER

Parameter	Value
DM Inductance	4×44.6 μH
DM Capacitance	2×150 nF
CM Inductance	1.68 mH
CM Capacitance	2×31.9nF
R_d Damping Resistor	33 Ω
Losses @ 230V	4.1 W
Size [mm]	36×39×11.4
Volume	16 cm^3

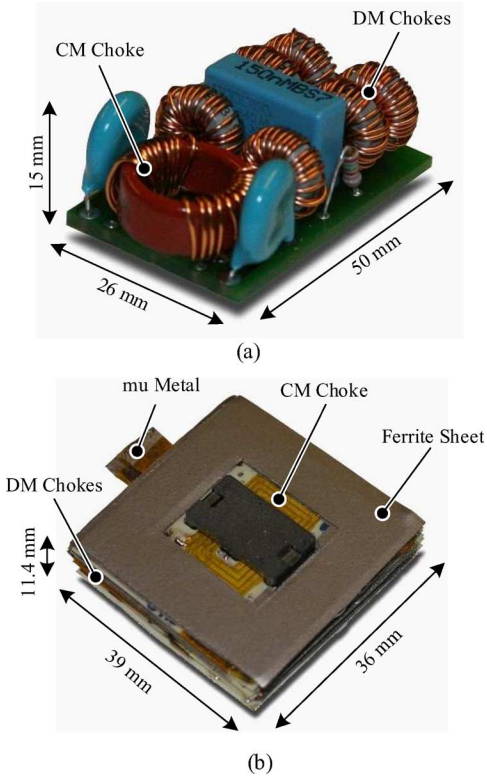

Fig. 19. (a) Photograph of the discrete and (b) the integrated EMI filter of a 300-W PFC. The integrated filter utilized an ELP22 core, the CM choke, and has in total eight 100 μ copper, two μ-metal, and four magnetic layers, where each inductor consists of only two copper layers instead of the four layers of the 600-W passive hybrid filter.

EMI filter for a 300-W PFC system. This PFC system is operating at a switching frequency of 200 kHz, and is designed for an output voltage of 400 V and an input voltage of 230 V (+10%/−15%). The parameters of the filter are given in Table VI, and in Fig. 19, photographs of the discrete and the integrated solution are given. The volume of the discrete filter is 22 cm^3, so that the volume could be decreased by 27% by integrating the filter in the PCB. This reduction is similar to the 600-W filter, where the volume could be shrunk by roughly 23% for the original design where ferrite foil has been utilized.

VI. CONCLUSION

The EMI filter is a significant part of a converter in terms of size and cost. Thus, the size of EMI filters must be reduced and the manufacturing simplified in order to increase the power density and reduce the cost of converter systems.

In this paper, a design procedure and measurement results for two different integration approaches—a passive hybrid integration in a PCB and an active hybrid integration with an active EMI filter—are presented. The filter inductors are integrated into a PCB board that could be manufactured with standard PCB manufacturing technology. Due to the integration, the filter volume could be reduced by approximately 40% while maintaining a high efficiency.

REFERENCES

[1] J. T. Strydom, "Electromagnetic design of integrated resonator-transformers," Ph.D. dissertation, Rand Afrikaans Univ., Johannesburg, South Africa, 2001.
[2] J. D. van Wyk, F. C. Lee, Z. Liang, R. Chen, S. Wang, and B. Lu, "Integrating active, passive and EMI-filter functions in power electronic system: A case study of some technologies," *IEEE Trans. Power Electron.*, vol. 20, no. 3, pp. 523–536, May 2005.
[3] E. Waffenschmidt, B. Ackermann, and J. A. Ferreira, "Design method and material technologies for passives in printed circuit board embedded circuits," *IEEE Trans. Power Electron.*, vol. 20, no. 3, pp. 576–584, May 2005.
[4] R. Chen, J. D. van Wyk, S. Wang, and W. G. Odendaal, "Improving the characteristics of integrated EMI filters by embedded conductive layers," *IEEE Trans. Power Electron.*, vol. 20, no. 3, pp. 611–619, May 2005.
[5] T. Farkas and M. F. Schlecht, "Viability of active EMI filters for utility applications," *IEEE Trans. Power Electron.*, vol. 9, no. 3, pp. 328–337, May 1994.
[6] L. Lawhite and M. F. Schlecht, "Design of active ripple filters for power circuits operating in the 1–10 MHz range," *IEEE Trans. Power Electron.*, vol. 3, no. 3, pp. 310–317, Jul. 1988.
[7] T. C. Neugebauer and D. J. Perrault, "Filters with inductance cancellation using printed circuit board transformers," *IEEE Trans. Power Electron.*, vol. 19, no. 3, pp. 591–602, May 2004.
[8] T. C. Neugebauer and D. J. Perrault, "Parasitic capacitance cancellation in filter inductors," in *Proc. 35th IEEE Power Electron. Spec. Conf. (PESC 2004)*, Aachen, Germany, Jun., pp. 3102–3107.
[9] M. J. Nave, "A novel differential mode rejection network for conducted emissions diagnostics," in *Proc. IEEE 1989 Nat. Symp. Electromagn. Compat.*, Denver, CO, May. 23–25,, pp. 223–227.
[10] M. L. Heldwein, T. Nussbaumer, F. Beck, and J. W. Kolar, "Novel three-phase CM/DM conducted emissions separator," in *Proc. 20th IEEE Annu. Appl. Power Electron. Conf. Expo.*, Austin, TX, Mar. 6–10, 2005, vol. 2, pp. 797–802.
[11] T. Nussbaumer, M. L. Heldwein, and J. W. Kolar, "Differential mode input filter design for a three-phase buck-type unity power factor PWM rectifier based on modeling of the EMC test receiver," *IEEE Trans. Ind. Electron.*, vol. 53, no. 5, pp. 1649–1661, Oct. 2006.
[12] M. Chen and J. Sun, "Low-frequency input impedance modeling of boost single-phase PFC converters," *IEEE Trans. Power Electron.*, vol. 22, no. 4, pp. 1521–1526, Jul. 2007.
[13] G. Spiazzi, L. Rossetto, and J. A. Pomilio, "Analysis of EMI filter induced instabilities in boost power factor preregulators," in *Proc. 29th IEEE Annu. Power Electron. Spec. Conf. (PESC 1998) Rec.*, May 17–22, vol. 2, pp. 1048–1053.
[14] [Online]. Available: http://www.epcos.de
[15] [Online]. Available: http://www.vacuumschmelze.de
[16] [Online]. Available: http://www.ohmega.com
[17] [Online]. Available: http://www2.dupont.com/Interra
[18] L. Oestergaard, "Modelling and simulation of the diode split transformer," Ph.D. dissertation, Faculty Eng. Sc., Aalborg Univ., Aalborg, Denmark, 1999, pp. 139–169.
[19] J. Biela and J. W. Kolar, "Using transformer parasitics for resonant converters—A review of the calculation of the stray capacitance of

transformers," in *Conf. Rec. 2005 IEEE Ind. Appl. Conf. 40th IAS Annu. Meeting*, Hong Kong, China, Oct. 2–6, vol. 3, pp. 1868–1875.

[20] M. L. Heldwein, H. Ertl, J. Biela, and J. W. Kolar, "Implementation of a transformer-less common mode active filter for off-line converter systems," in *Proc. 21th Annu. IEEE Appl. Power Electron. Conf. Expo. (APEC)*, Dallas, TX, Mar. 19–23, 2006, p. 7.

Juergen Biela (S'04–M'06) received the diploma (with honours) from the Friedrich-Alexander University in Erlangen, Germany in 2000 and the Ph.D. degree from ETH Zurich in 2005, all in electrical engineering. In the course of his M.Sc. studies he dealt in particular with resonant DC-link inverters at the Strathclyde University, Scotland (term project) and the active control of series connected IGCTs at the Technical University of Munich (diploma thesis).

He has worked at the research department of A&D Siemens, Germany, from 2000 to June 2001, where he focused on inverters with very high switching frequencies, SiC components and EMC. In July 2002, he joined the Power Electronic Systems Laboratory (PES), ETH Zurich, to work toward the Ph.D. degree, concentrating on optimized electromagnetically integrated resonant converters. From 2006 to 2007 he was a Post-Doctoral Fellow with PES and has been a guest researcher at the Tokyo Institute of Technology, Japan. Since 2007 he is working as Senior Research Associate at PES, ETH Zurich.

His current research interest include multi-domain modelling, design and optimization of power electronic systems, in particular systems for future energy distribution and pulsed power applications, advanced power electronic systems based on novel semiconductor technologies and integrated passive components for ultra compact and ultra efficient converter systems.

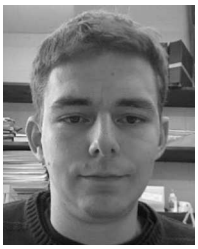

Alexander Wirthmueller was born in Regensburg, Germany, on February 13, 1982. He has been studying electrical engineering at the Swiss Federal Institute of Technology Zurich (ETH Zurich), Zurich, Switzerland, since October 2002. He is currently working toward the Diploma in silicon photonics at Columbia University, New York.

His research interests include the design of integrated passives for power electronics applications as well as with quantum transport simulation in semiconductor devices.

Roman Waespe was born in Zurich, Switzerland, on August 12, 1982. He received the Diploma degree in distributed generation integration from the University of Canterbury, Christchurch, New Zealand, in 2007, and has been studying electrical engineering at the Swiss Federal Institute of Technology Zurich (ETH Zurich), Zurich, Switzerland, since October 2002.

He is currently with the Power Electronic Systems Laboratory, ETH Zurich. His research interests include the design of integrated passives for power electronics as well as with real-time imaging processing algorithms.

Marcello Lobo Heldwein (S'99–M'06) received the B.S. and M.S. degrees in electrical engineering from the Federal University of Santa Catarina, Florianópolis, Brazil, in 1997 and 1999, respectively, and the Ph.D. degree from the Swiss Federal Institute of Technology (ETH Zurich), Zurich, Switzerland, in 2007.

He is currently working as a Postdoctoral Fellow at the Power Electronics Institute (INEP), Federal University of Santa Catarina (UFSC), Florianópolis, Brazil. From 1999 to 2001, he was a R&D engineer with the Power Electronics Institute, Federal University of Santa Catarina. From 2001 to 2003, he was an Electrical Design Engineer with Emerson Energy Systems, in São José dos Campos, Brazil and in Stockholm, Sweden. His current research interests include power factor correction techniques, static power converters, multilevel converters and EMC for power electronics.

Mr. Heldwein is currently a member of the Brazilian Power Electronic Society (SOBRAEP) and of the IEEE.

Klaus Raggl was born in Zams, Austria, in 1980. He received the M.Sc. degree in mechatronics from Johannes Kepler University Linz, Linz, Austria, in 2005, and the Ph.D. degree in 2009 from the Power Electronic Systems Laboratory (PES), Swiss Federal Institute of Technology (ETH) Zurich, Zurich, Switzerland, in 2009.

At ETH Zurich, he worked on bearingless pump systems with high power density, section drive technology, and magnetic bearings. Since April 2009, he has been with Hilti AG, Schaan, Liechtenstein, where he is working on high-performance drilling and demolition machines.

Johann W. Kolar (M'89–SM'02) received the Ph.D. degree (*summa cum laude*) from the University of Technology Vienna, Vienna, Austria, where he studied industrial electronics.

From 1984 to 2001, he was with the University of Technology Vienna, where he was teaching and engaged in research in close collaboration with the industry. He has proposed numerous novel converter topologies, e.g., the VIENNA rectifier and the three-phase ac-ac sparse matrix converter concept. He is the author or coauthor of more than 200 scientific papers in international journals and conference proceedings, and has filed more than 50 patents. In February 2001, he was appointed a Professor and the Head of the Power Electronics Systems Laboratory, Swiss Federal Institute of Technology Zurich, (ETH Zurich), Zurich, Switzerland. His current research interests include ultracompact intelligent ac–ac and dc–dc converter modules employing latest power semiconductor technology (SiC), novel concepts for cooling and active electromagnetic interference (EMI) filtering, multidisciplinary simulation, bearingless motors, power microelectromechanical systems (MEMS), and wireless power transmission.